IOPscience iopscience.iop.org

Home Search Collections Journals About Contact us My IOPscience

Synthesis, characterization and electrical properties of the new solid electrolyte materials $Ce_{6-x}Er_xMoO_{15-\delta}$ ($0.0 < x < 1.5$)

This article has been downloaded from IOPscience. Please scroll down to see the full text article.

2003 J. Phys.: Condens. Matter 15 5181

(http://iopscience.iop.org/0953-8984/15/29/329)

View the table of contents for this issue, or go to the journal homepage for more

Download details:
IP Address: 171.66.16.121
The article was downloaded on 19/05/2010 at 14:21

Please note that terms and conditions apply.

INSTITUTE OF PHYSICS PUBLISHING JOURNAL OF PHYSICS: CONDENSED MATTER

J. Phys.: Condens. Matter **15** (2003) 5181–5190 PII: S0953-8984(03)60991-4

Synthesis, characterization and electrical properties of the new solid electrolyte materials $Ce_{6-x}Er_xMoO_{15-\delta}$ ($0.0 < x < 1.5$)

Qibing Bo, Jing Feng, Ping Che, Jinping Wang, Qiuyan Wang, Xueqiang Cao and Jian Meng[1]

Key Laboratory of Rare Earth Chemistry and Physics, Changchun Institute of Applied Chemistry, Chinese Academy of Sciences, Changchun 130022, Jilin, China

E-mail: jmeng@ns.ciac.jl.cn

Received 18 March 2003
Published 11 July 2003
Online at stacks.iop.org/JPhysCM/15/5181

Abstract

A new series of oxides, $Ce_{6-x}Er_xMoO_{15-\delta}$ ($0.0 \leqslant x < 1.5$), was synthesized using wet-chemistry techniques. The precursors and resultant oxide powders were characterized by differential thermal analysis/thermogravimetry, x-ray diffraction, and IR, Raman and x-ray photoelectron spectroscopy. The formation temperature of the powders was found to be as low as 350 °C. $Ce_{6-x}Er_xMoO_{15-\delta}$ crystallized to a fluorite-related cubic structure. The electrical conductivity of the samples was investigated by using ac impedance spectroscopy. This showed that the presence of Er was related to the oxygen-ion conductivity, and that the highest oxygen-ion conductivity was found in $Ce_{6-x}Er_xMoO_{15-\delta}$ ($x = 0.4$), ranging from 5.9×10^{-5} S cm^{-1} at 300 °C to 1.26×10^{-2} S cm^{-1} at 700 °C, respectively. This kind of material shows a potential application in intermediate-temperature solid oxide fuel cells.

(Some figures in this article are in colour only in the electronic version)

1. Introduction

Oxide ion conductors are important functional materials that can be used as electrolytes for fuel cells, oxygen sensors, and films for separating oxygen from air [1]. The most successful oxide electrolytes have been those based on one of the oxides ZrO_2 [2], Bi_2O_3 [3], CeO_2 [4], $LaGaO_3$ [5] and La_2GeO_5 [6]. But traditional solid oxide fuel cells (SOFCs), which use the electrolytes above, usually require a high operating temperature (e.g. 1000 °C) to achieve high ionic conductivity. Lowering the operating temperature would prolong lifetime threefold and reduce material and production costs. But a lot of research work has now been undertaken to

[1] Author to whom any correspondence should be addressed.

 © 2003 IOP Publishing Ltd Printed in the UK

tailor advanced materials that would allow operation at lower temperatures, typically in the range of 500–800 °C. Recently, Lacorre *et al* reported an attractive oxide ion conductivity of $La_2Mo_2O_9$. At 580 °C, this undergoes a monoclinic-to-cubic first-order phase transition, accompanied by an increase in the ionic conductivity of two orders of magnitude [7].

Here, we report the novel oxide Ce_6MoO_{15} and its physical properties. The x-ray diffraction (XRD) spectra showed that it is similar to that of CeO_2, and that all of its peaks can be indexed on the basis of cubic fluorite-related type structures. We found that it has high oxygen-ion conductivity at intermediate temperatures. To enhance its conductive performance, we substituted Ce with Er and obtained a new series of oxygen-ion conducting oxides, $Ce_{6-x}Er_xMoO_{15-\delta}$. The figure of merit of $Ce_{6-x}Er_xMoO_{15-\delta}$ (for $x = 0.4$) is 1.26×10^{-2} S cm^{-1} at 700 °C.

2. Experimental section

Compounds of the general formula $Ce_{6-x}Er_xMoO_{15-\delta}$ ($0.0 \leqslant x < 1.5$) were prepared using a modified sol–gel method, as reported in the literature elsewhere [8, 9]. Erbium and cerium nitrates and ammonium molybdate $(NH_4)Mo_7O_{24}{\cdot}6H_2O$ solutions were prepared separately and then mixed according to the stoichiometric ratios of the samples. Suitable citric acid and polyethylene glycol 20 000 solutions were then added slowly to the mixture under constant stirring. The pH value of the solution was adjusted to the required level with the addition of ammonia or nitric acid. The solution was vapourized using a water bath at 60–70 °C, becoming a transparent sol then a gel. The gel was dried at 110 °C. Dried gel was then calcined at various temperatures in air and cooled to room temperature.

Differential thermal analysis/thermogravimetry (DTA/TG) were carried out on an SDT 2960 (TA Instruments), with a heating temperature changing at 7 °C min^{-1} from 20 to 800 °C, in air. XRD patterns for all the samples were recorded on a Rigaku D/max-IIB x-ray diffractometer using Cu Kα_1 radiation ($\lambda = 1.5405$ Å) with silicon powder as the internal standard. Structural analysis software called CELL, written by Takaki *et al* [10] was used to refine the precise structural parameters. IR spectra were recorded at room temperature with a Bio-Rad FTS spectrometer. Raman spectra were taken in the quasi-backscattering geometry using 100 mW of the 5145 Å line of an argon ion laser as the excitation source; both the spectral resolution and the accuracy in the Raman shift were estimated to be $\sim$2 cm^{-1}. XPS spectra for powder samples were measured on an EXCA-LAS MK II x-ray photoelectron spectrometer from VG using Al Kα radiation; the base pressure was 10^{-7} Pa, and the C_{1s} signal was used to correct the charge effects on the sample surface.

The final oxide powders for conductivity measurement were pressed into disks of 15 mm diameter, then sintered in air at 1400 °C for 8 h, polished to a disk (of about 12 mm in diameter and 2–3 mm in thickness) and coated with platinum as an electrode material using an SC-701 quick coater apparatus from Sanyu Denshi Co Ltd. Oxide ionic conductivity was measured at different temperatures by a conventional ac two-probe technique using a frequency response analyser (Solatron 1255) and an electrochemical interface (SI1287) controlled by a personal computer in a frequency range from 1.0×10^6 to 0.1 Hz. The temperature was controlled by a ÜGU-808P temperature controller. A 50 min interval was allowed for thermal stabilization after each temperature change. Curve fitting and resistance estimation were performed by using Zview software[2].

[2] Zview (ver.1.2) 1994 *Impedance/Gain Phase Graphics and Analysis Software* Scribner Associates.

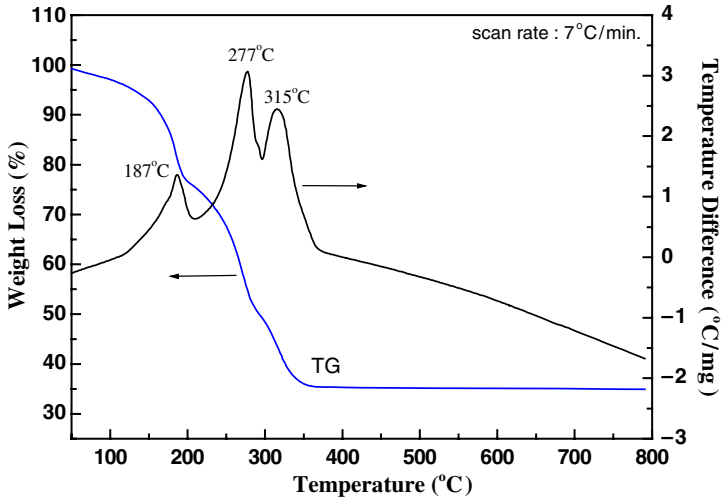

Figure 1. The simultaneous DTA/TG curves of the sample $Ce_{6-x}Er_xMoO_{15-\delta}$ ($x = 0.4$) dried at 110 °C.

3. Results and discussion

3.1. Thermal analysis

Clear thermal events corresponding to the crystallization process of a sample were identified in the thermal analysis. Figure 1 shows the DTA/TG curves of the $Ce_{6-x}Er_xMoO_{15-\delta}$ ($x = 0.4$) precursor dried at 110 °C. With a weakly exothermic peak, the TG curve reveals a weight loss of 22.49% below 200 °C, which corresponds to the complete decomposition of citrate or citric acid monohydrate. At the same time, there are two exothermic peaks at 277 and 315 °C, accompanied by 25.75 and 15.97% weight losses, respectively, which suggests that the polymer between the metal ion and citric acid monohydrate or polyethylene glycol 20 000 decomposes. From 350 to 800 °C, no change in weight was found, indicating that the single phase of a sample may be formed at 350 °C. This has been evidenced by XRD results, as shown in figure 2.

3.2. XRD

We have undertaken a systematic study of the phase evolution of the $Ce_{6-x}Er_xMoO_{15-\delta}$ ($x = 0.4$) precursor during calcination. The precursor was calcined at a selected temperature for 8 h in air and then subjected to XRD analysis after cooling to room temperature (figure 2). It was found that the precursor is amorphous below 300 °C. When the temperature reaches 350 °C, the sample has already displayed almost all the characteristic reflections, like the cubic structure of CeO_2. Above 350 °C, no other crystalline phases were detected along with the cubic-structure solid solution. The facts indicate that the formation temperature of the single-phase sample is as low as 350 °C, which is in accord with the results of the thermal analysis above. Meanwhile, with an increase in the thermal treatment temperature, the peaks of the crystalline samples gradually sharpen, indicating better crystallization of the particles and an increase in particle size.

The substitution of Er^{3+} for Ce^{4+} was tried systematically, to observe the change in the crystalline structure. The XRD patterns of the solid solution of CeO_2 and $Ce_{6-x}Er_xMoO_{15-\delta}$

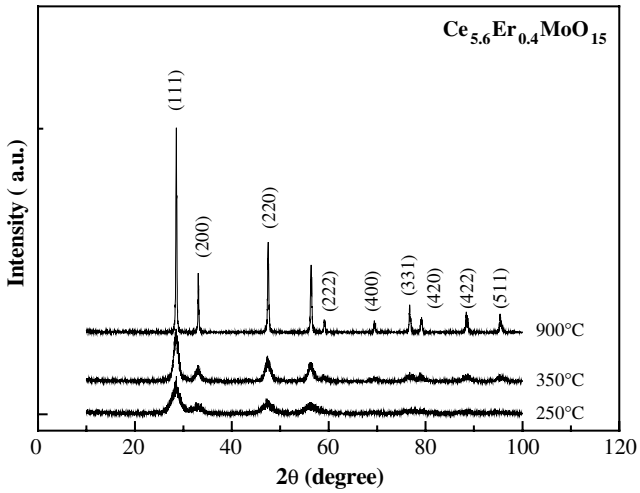

Figure 2. The XRD patterns of $Ce_{6-x}Er_xMoO_{15-\delta}$ ($x = 0.4$) precursors calcined at different temperatures: (a) 250 °C, (b) 350°C and (c) 900 °C.

Table 1. The unit cell parameters indexed on the cubic lattice.

Sample composition	Lattice parameters[a] a (Å)	V(Å^3)
$Ce_{5.9}Er_{0.1}MoO_{15-\delta}$	5.4126 ± 0.0002	158.5688
$Ce_{5.8}Er_{0.2}MoO_{15-\delta}$	5.4123 ± 0.0002	158.5425
$Ce_{5.7}Er_{0.3}MoO_{15-\delta}$	5.4121 ± 0.0003	158.5249
$Ce_{5.6}Er_{0.4}MoO_{15-\delta}$	5.4113 ± 0.0002	158.4546
$Ce_{5.5}Er_{0.5}MoO_{15-\delta}$	5.4112 ± 0.0004	158.4458
$Ce_{5.4}Er_{0.6}MoO_{15-\delta}$	5.4093 ± 0.0002	158.2790
$Ce_{5.2}Er_{0.8}MoO_{15-\delta}$	5.4072 ± 0.0002	158.1035
$Ce_{5.0}Er_{1.0}MoO_{15-\delta}$	5.4036 ± 0.0004	157.7791
$Ce_{4.8}Er_{1.2}MoO_{15-\delta}$	5.3997 ± 0.0002	157.4378
$Ce_{4.6}Er_{1.4}MoO_{15-\delta}$	5.3970 ± 0.0002	157.2045

[a] Indexed by the CELL program [10].

($x = 0.0$–1.4) sintered at 900 °C are given in figure 3. By using the CELL software we were able to index all the diffraction lines with the primitive cubic-fluorite unit cell. All the powders were single-phase fluorite structures. However, impurities were detected by XRD analysis above $x > 1.4$ in $Ce_{6-x}Er_xMoO_{15-\delta}$. Therefore, it is concluded that the limit of the solid solution of doped-Er is at about $x = 1.4$. All the lattice constants refined by x-ray powder diffraction analysis decreased linearly with an increase in the Er content, as shown in table 1. This indicated that Er had dissolved into the Ce sites in Ce_6MoO_{15} and isostructural phases had been formed.

3.3. XPS

To probe the valence distribution in the solid solution Ce_6MoO_{15} sintered at 900 °C, XPS spectra were measured at room temperature using the standard CeO_2 as a reference. The core level spectra of Ce_{3d} and Mo_{3d} are illustrated in figure 4. The $Ce3d_{5/2}$ signals consist of photoelectron peaks at (a) 882.2 eV and (b) 882.1 eV for Ce_6MoO_{15} and the standard CeO_2, respectively. All the observed peaks could be assigned to Ce^{4+} species by comparison with

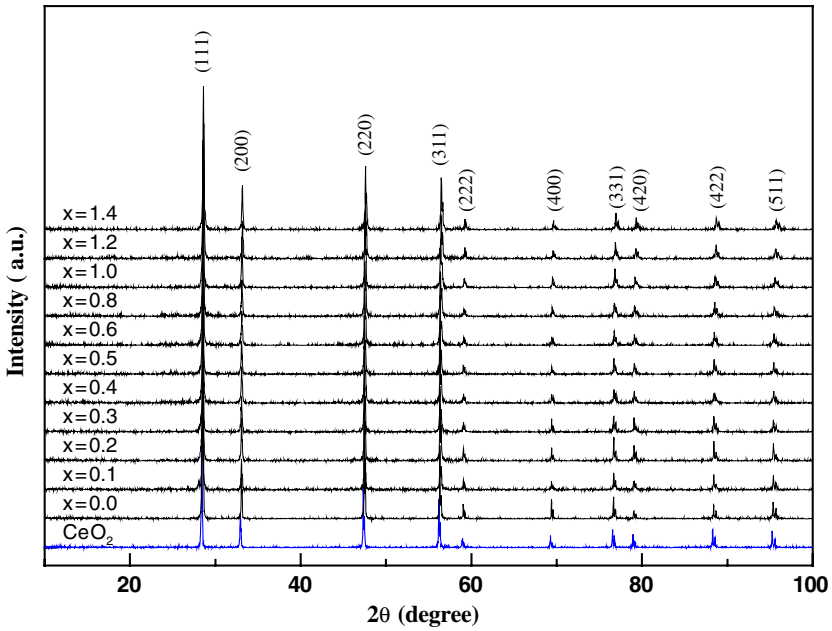

Figure 3. The XRD patterns of CeO_2 and $Ce_{6-x}Er_xMoO_{15-\delta}$ calcined at 900 °C ($x = 0.0$–1.4).

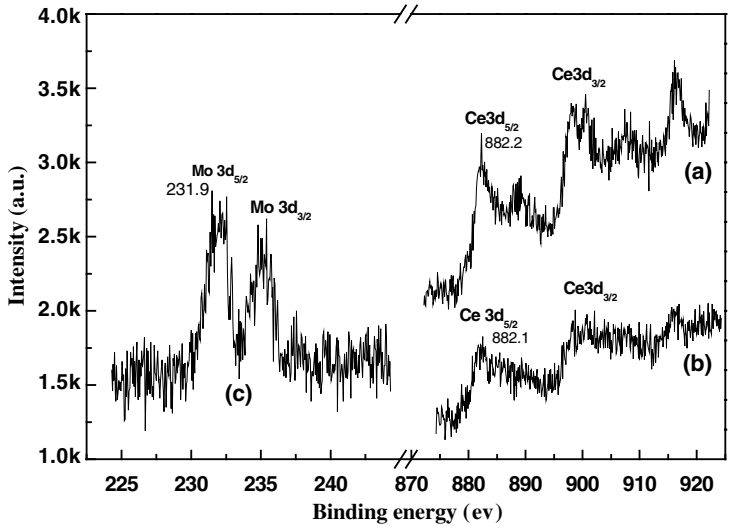

Figure 4. XPS of Ce_{3d} for (a) CeO_2 and (b) Ce_6MoO_{15} and of Mo_{3d} for (c) Ce_6MoO_{15}.

the data reported in the literature [11, 12]; no signals relative to Ce^{3+} species are observed in the spectra. The other spectrum was obtained for (c) $Mo3d_{5/2}$ (231.9 eV) from Ce_6MoO_{15}, which is invariably characteristic of the (VI) oxidation state [13, 14]. So, the experimental results confirmed that only Ce^{4+} and Mo^{6+} exist in solid solution. According to the principle of charge balance, the defined chemical formula Ce_6MoO_{15} is correct.

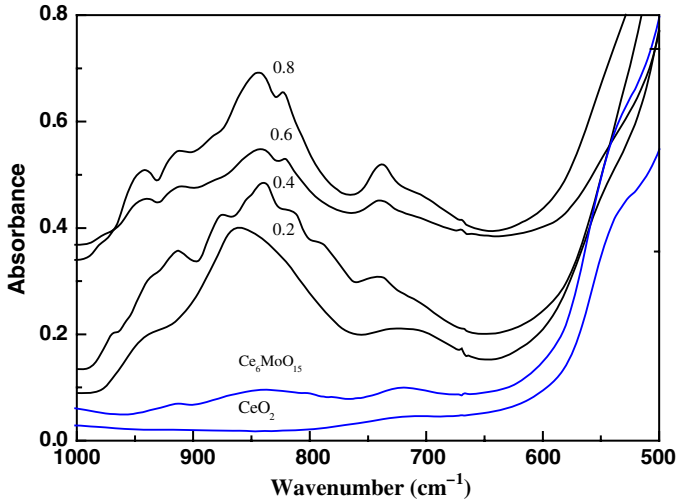

Figure 5. IR absorption spectra of CeO_2, Ce_6MoO_{15} and (c) $Ce_{6-x}Er_xMoO_{15-\delta}$ (for x = 0.2, 0.4, 0.6, 0.8).

3.4. IR

All the IR spectra of $Ce_{6-x}Er_xMoO_{15-\delta}$ are similar. Here, a typical IR spectrum of compounds Ce_6MoO_{15} and $Ce_{6-x}Er_xMoO_{15-\delta}$ (x = 0.2, 0.4, 0.6, 0.8) is given in figure 5. Here, CeO_2 is presented for comparison. From the IR spectra it is clear that only an absorption band around 725 cm^{-1} was observed in CeO_2, which corresponds to Ce–O stretching modes [15]. Characteristic bands at 920 and 833 cm^{-1} confirmed the formation of the [MoO_6] octahedral in Ce_6MoO_{15} according to data in the literature [16–18]. With increasing Er doping content, it is seen that the vibration at 725 cm^{-1}, which exists in CeO_2, shifts to a higher frequency, accompanied by a small band at 680 cm^{-1}, due to lower symmetry than that in CeO_2. These facts indicated that Er had entered the Ce sites to form solid solutions of $Ce_{6-x}Er_xMoO_{15-\delta}$. At the same time, the bands between 930 and 970 cm^{-1} in $Ce_{6-x}Er_xMoO_{15-\delta}$ are assigned to the Mo=O vibration, while the shoulder below 900 cm^{-1} (820–880) is ascribed to vibrations along Mo–O–Mo bridges. This confirmed that parts of the [MoO_4] tetrahedral appeared in $Ce_{6-x}Er_xMoO_{15-\delta}$, in accord with [16].

3.5. Raman spectra

Tentative information has been obtained by comparing samples by means of Raman spectra, since no structural information is available on the above-mentioned crystalline ternary Ce–Mo–Er phases. The room-temperature Raman spectra for the compounds CeO_2, Ce_6MoO_{15} and $Ce_{6-x}Er_xMoO_{15-\delta}$ (x = 0.2, 0.4, 0.6, 0.8) are shown in figure 6. It is evident that a peak at about 464 cm^{-1} in CeO_2 and Ce_6MoO_{15} is ascribed to the Raman-active F_{2g} symmetry mode of the typical fluorite metal dioxides [19]. With an increasing level of Er doping, different spectra appeared. All the spectra show some similarity, with a number of overlapping bands in the spectral range 100–700 cm^{-1} as a dominant feature. Perhaps this effect of a change in the vibration frequency can be viewed as a result of the influence of the smaller number of Er ions on the [MoO_6] groups, similar to the conclusion drawn from the IR spectra.

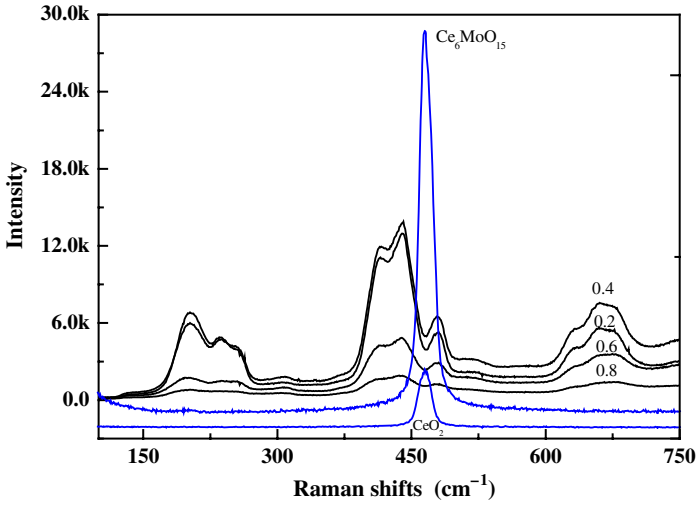

Figure 6. Raman spectra of CeO_2, Ce_6MoO_{15} and $Ce_{6-x}Er_xMoO_{15-\delta}$ ($x = 0.2, 0.4, 0.6, 0.8$).

3.6. ac impedance spectroscopy

The method of impedance spectroscopy is a powerful technique for investigating the electrical properties of solid electrolytes. ac impedance spectroscopy normally allows the separation of bulk, grain-boundary and electrode processes in ceramic samples [20]. Figure 7 shows an impedance spectrum for $Ce_{6-x}Er_xMoO_{15-\delta}$ ($x = 0.4$) at various temperatures, where R_b is the bulk resistance of the sample and R_{gb} is the resistance associated with the grain boundary. At moderate temperatures, such as 300 °C, the spectrum of the sample consisted of two depressed semi-circles and a spike. The high-frequency semi-circle originates from the bulk transport, the lowest-frequency spike is due to oxide-ion transfer at the electrode, and the intermediate-frequency semi-circle gives information on the grain-boundary resistance to oxide-ion motion. Looking carefully at figure 7, all of the semi-circles appear depressed, which is attributed to the constant phase element (CPE) parameter [21]. From the viewpoint of thermodynamics, at low temperatures (such as 300 °C) this involves an infinite diffusion process between the electrode and the sample because the mobility of the charge carriers is limited. As a result, a spike appears at low frequency. On the other hand, the microstructure of the sample can be treated as an array of cubic-shaped grains, which are separated by flat grain boundaries. With an increase in temperature, the charge carrier in the grain moves easily through the diffusion process, then the grain boundary process becomes weaker and the spike is attributed to the process of the electrode/electrolyte interface being bent down. Finally, only two semi-circles exist. These facts indicated that R_{gb} decreased and the reversibility of the charge migration processes of the electrode/electrolyte interface increased. Therefore, it is easy to separate the resistance R_b and that of the grain boundary R_{gb} from figure 7. The total resistance was then conveniently converted to electrical conductivity (σ) by considering the thickness and area of the sample.

3.7. Electrical conductivity

Figure 8 shows the effects on the electrical conductivity in air of Er substitution for the Ce sites in Ce_6MoO_{15}. It should be noted that, for reasons of clarity, only a partial selection of samples

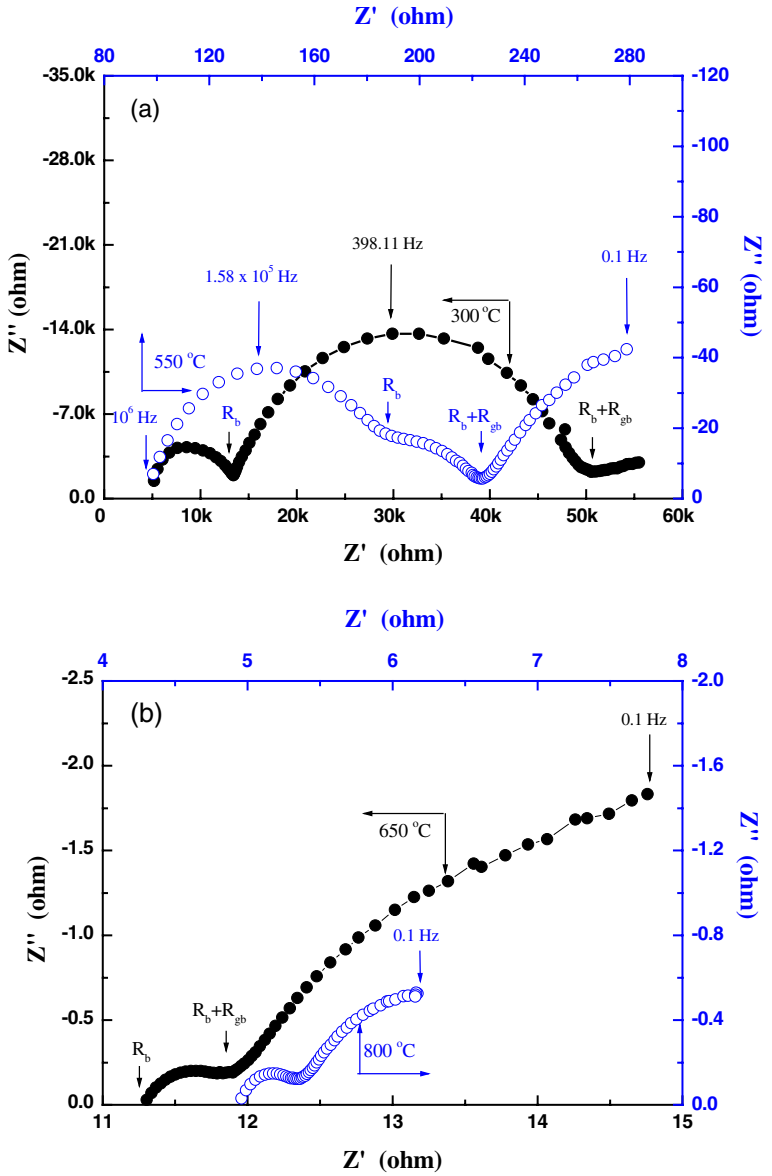

Figure 7. The ac impedance spectra of $Ce_{6-x}Er_xMoO_{15-\delta}$ ($x = 0.4$) at (a) 300 and 550 °C and (b) 650 and 800 °C.

has been included in figure 8. We notice that the Arrhenius plot of conductivity is curved, dividing into two straight-line regions above and below a transition temperature $T^* = 600$ °C. This behaviour is well-described by a model in which all the oxygen vacancies are mobile at temperature $T > T^*$ but progressively condense into clusters of ordered vacancies with decreasing temperature $T < T^*$. On the other hand, the electrical conductivity seems to fall into two distinct regions with the increase in dopant content. When $0 < x < 0.5$, the conductivity in $Ce_{6-x}Er_xMoO_{15-\delta}$ increased with an increase in the amount of Er additives and attained a maximum at $x = 0.4$. Since the number of oxide vacancies increases with

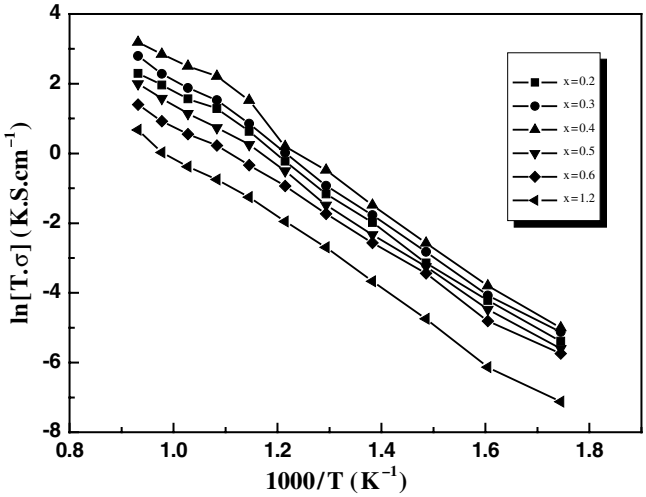

Figure 8. The temperature dependence of conductivity for $Ce_{6-x}Er_xMoO_{15-\delta}$.

an increase in Er dopant, theoretically larger numbers of oxide vacancies are obtained. As a result, higher oxide-ion conductivity is consistent with larger amounts of Er dopant. However, the conductivity of the samples with high Er content ($0.4 < x < 1.4$) is lower than that of the samples with low Er content ($0 < x < 0.5$). This is possibly due to oxygen vacancy clustering or the severe lattice deformation in doped samples. As a result, this impedes the mobility of oxygen vacancies. Consequently, to obtain very high ionic conductivity, the optimum amount of additional Er for the Ce site seems to be $x = 0.4$.

4. Conclusions

By using the soft-chemical method we have successfully synthesized a type of novel solid solution, $Ce_{6-x}Er_xMoO_{15-\delta}$, based on Ce_6MoO_{15}. The formation temperature of the samples is as low as 350 °C. Single-phase samples became difficult to obtain when the amount of Er reaches $x > 1.4$. Structural characterization shows that the new compound Ce_6MoO_{15} and its Er-doped samples have cubic fluorite-type structures, and that the [MoO_6] octahedra units remaining in Ce_6MoO_{15} were affected by the doping of Er. The variation in the lattice parameter is in agreement with that of the ionic radius of the dopants. Solid solution $Ce_{6-x}Er_xMoO_{15-\delta}$ ($x = 0.4$) has the highest oxygen-ion conductivity compared with the others, showing that it has a potential application in SOFCs.

Acknowledgments

This work was supported by the State Key Program of Basic Research of China (G1998061311) and the National Natural Science Foundation of China (20271049).

References

[1] Boivin J C and Mairesse G 1998 *Chem. Mater.* **10** 2870
[2] Kharton V V, Naumovich E N and Vecher A A 1999 *J. Solid State Electrochem.* **3** 61
[3] Kharton V V, Naumovich E N, Yaremchenko A A and Marques F M B 2001 *J. Solid State Electrochem.* **5** 160

[4] Inaba H and Tagawa H 1996 *Solid State Ion.* **83** 1
[5] Ishihara T, Matsuda H and Takita Y 1994 *J. Am. Chem. Soc.* **116** 3801
[6] Ishihara T, Arikawa H, Akbay T, Nishiguchi H and Takita Y 2001 *J. Am. Chem. Soc.* **123** 203
[7] Lacorre P, Goutenoire F, Bolmke O, Retoux R and Laligant Y 2000 *Nature* **404** 856
[8] Lakeman C D E and Payne D A 1994 *Mater. Chem. Phys.* **38** 305
[9] Marcilly C, Courty P and Delmon B 1970 *J. Am. Ceram. Soc.* **53** 56
[10] Takaki Y, Taniguchi T and Hori K 1993 *J. Ceram. Soc. Japan* **101** 373
[11] Nefedov V I, Gati D, Dzhurinskii B F, Sergushin N P and Salyn Y V 1975 *Zh. Neorg. Khim.* **20** 2307
[12] Barr T L, Fries C G, Cariati F, Bart J C J and Giordano N 1983 *J. Chem. Soc. Dalton Trans.*
[13] Cimino A and De Angelis B A 1975 *J. Catal.* **36** 11
[14] Caceres C V, Fierro J L G, Lazaro J, Agudo A L and Soria J 1990 *J. Catal.* **122** 113
[15] Nyquist R A and Kagel R O 1971 *Infrared Spectra of Inorganic Compounds* (New York: Academic) p 228
[16] Bart J C J, Forzatti P, Garbassi F and Cariati F 1987 *Z. Anorg. Allg. Chem.* **546** 206
[17] Clark G M and Doyle W P 1966 *Spectrochim. Acta* **22** 1441
[18] Busey R H and Keller O L 1964 *J. Chem. Phys.* **41** 215
[19] McBride J R, Hass K C, Poindexte B D and Weber W H 1994 *J. Appl. Phys.* **76** 2435
[20] Bauerle J E 1969 *J. Phys. Chem. Solids* **30** 2657
[21] Ross Macdonald J 1987 *Impedance Spectroscopy—Emphasizing Solid Materials and Systems* (New York: Wiley) p 91